Motion-Driven Flow in an Unusual Piscine Nasal Region

Mawuli P. K. Agbesi[a], Heather S. Borsuk[a], Jeremy N. Hunt[b], James S. Maclaine[c], Richard L. Abel[d,1], Dan Sykes[d,2], Andrew T. Ramsey[e], Zhijin Wang[a], Jonathan P. L. Cox[f,*]

[a]Department of Mechanical Engineering, University of Bath, Bath, BA2 7AY, UK
[b]Jeremy Hunt Design, Unit A6, 66 Norlington Road, London, E10 6LA, UK
[c]Department of Life Sciences, Natural History Museum, Cromwell Road, London, SW7 5BD, UK
[d]Imaging and Analysis Centre, Natural History Museum, Cromwell Road, London, SW7 5BD, UK
[e]Nikon Metrology, Icknield Way, Tring, Hertfordshire HP23 4JX, UK
[f]Department of Chemistry, University of Bath, Bath, BA2 7AY, UK

[*]Corresponding author. Tel.: +44 1225 386548

E-mail address: j.p.l.cox@bath.ac.uk

[1] Present address: Department of Surgery and Cancer, Imperial College, London, W6 8RF, UK.
[2] Present address: Henry Moseley X-ray Imaging Facility, University of Manchester, Manchester, M13 9PY, UK.

ABSTRACT

Fishes have several means of moving water to effect odorant transport to their olfactory epithelium ('olfactory flow'). Here we show that olfactory flow in the adult garpike *Belone belone* (Belonidae, Teleostei), a fish with an unusual nasal region, can be generated by its motion relative to water (swimming, or an external current, or both). We also show how the unusual features of the garpike's nasal region influence olfactory flow. These features comprise a triangular nasal cavity in which the olfactory epithelium is exposed to the external environment, a papilla situated within the nasal cavity, and an elongated ventral apex. To perform our investigation we first generated life-like plastic models of garpike heads from X-ray scans of preserved specimens. We then suspended these models in a flume and flowed water over them to simulate swimming. By directing filaments of dye at the static models, we were able to visualise flow in the nasal regions at physiologically relevant Reynolds numbers (700 – 2,000). We found that flow of water over the heads did cause circulation in the nasal cavity. Vortices may assist in this circulation. The pattern of olfactory flow was influenced by morphological variations and the asymmetry of the nasal region. The unusual features of the nasal region may improve odorant sampling in the garpike, by dispersing flow over the olfactory epithelium and by creating favourable conditions for odorant transport (e.g. steep velocity gradients). Unexpectedly, we found that the mouth and the base of the garpike's jaws may assist the sampling process. Thus, despite its apparent simplicity, the garpike's nasal region is likely to act as an effective trap for odorant molecules.

Keywords: Beloniform, fluid dynamics, needlefish, olfaction, X-ray microcomputed tomography.

1. Introduction

Perception of smell in water requires transport of odorant molecules from the animal's external environment to its olfactory epithelium. Because diffusion times in water are extremely long (Denny, 1993, Fig. 6.3), aquatic animals *must* in the first instance rely on the bulk movement of water for odorant transport (Cox, 2008, p. 579 and 581). The final stage of this process, however, involves diffusion alone (Vogel, 1994, pp. 196-197).

In fishes, four principal mechanisms may be used to generate bulk movement of water in the nasal region ('olfactory flow'): 1) the beating of non-sensory cilia; 2) the expansion and contraction of accessory sacs; 3) respiration; and 4) the movement of the fish relative to water (Cox, 2008). Mechanical agitation of the nasal region may also contribute to olfactory flow, but in a non-directional manner (Cox, 2008, p. 583). Which mechanism(s) operate(s) depends on the species of fish.

Our aim here was to investigate olfactory flow in the adult garpike, *Belone belone* (Belonidae, Beloniformes, Teleostei). The garpike is a long, slender, marine fish with beak-like jaws (Figs. 1 and 2; Wheeler, 1969, pp. 236-237). Its elongated body, together with its prominent tail and the extreme posterior positioning of its dorsal and anal fins (Fig. 1), suggests that it is an active swimmer (Helfman et al., 2009, Table 8.1). Indeed, according to Theisen et al. (1980, p. 169), adult garpike are known to swim 'continuously and normally rather fast'.

The garpike has an unusual nasal region (Fig. 3). The olfactory epithelium of most non-beloniform fishes is enclosed in a nasal chamber, and is typically located on one or more thin folds, or lamellae (Hara, 1975; Zeiske et al., 1992; Cox, 2008). But, in the garpike, the olfactory epithelium is largely exposed to the external environment: it lines a triangular nasal cavity (Fig. 3B, NC) and the surface of a papilla situated within the nasal cavity (Fig. 3B, Pp; Blaue, 1884, pp. 241-245 and Figs. 1-3; Burne, 1909, Fig. 203A; Theisen et al., 1980, Fig. 2; Cox, 2008, Fig. 3). The nasal cavity widens caudally and its edges are sharp. There is a recess beneath the dorsal edge (Fig. 3C, Re). The ventral apex may be somewhat elongated (Fig. 3B, VA).

Olfactory flow in the garpike is likely to be generated primarily by its motion relative to water. Given that adult garpike are likely to be active swimmers, we assume that swimming is the main source of this motion, although an oncoming current could augment olfactory flow. Olfactory flow cannot be generated by the beating of non-sensory cilia, because the nasal region of the adult garpike lacks ciliated non-sensory cells (Theisen et al., 1980, p. 167). Nor can it be generated by accessory sacs, as the garpike also lacks these anatomical devices. Some olfactory flow could be generated by respiration (the paired nasal regions are situated close to the mouth; Fig. 2), or mechanical agitation of the nasal region (e.g. by movement of the jaws). Mechanical agitation is likely to make only a minor contribution to olfactory flow given that other belonids typically swim with their jaws closed (B. Collette, personal communication).

In undertaking this study, we had two objectives. First, we wanted to demonstrate that olfactory flow in the garpike can be generated by swimming. Second, we wanted to determine how the unusual features of the garpike's nasal region (nasal cavity, papilla, ventral apex) influenced olfactory flow and the likely effect of these influences on odorant sampling in the garpike. As a subject for studying olfactory flow, the garpike appealed for several, mainly practical, reasons. First, swimming could be simulated by flowing water over a static, life-like, plastic model of the garpike's head. Moving fluid over a static model, a valid device that is also used to simulate flow over, for example, aircraft (Shapiro, 1961, p. 77), is equivalent to moving the model through static water, but easier to achieve. Second, the garpike's nasal region does not possess any moving parts that might complicate olfactory flow (e.g. the flexible lamellae typical of the nasal regions of other fishes). The rigidity of the nasal region could therefore be replicated in the plastic model. Third, the exposed nasal region allows direct observation of olfactory flow. Fourth, there is only one previous study of olfactory flow in the garpike, and this was mentioned only in passing (Zeiske and Hansen, 2005, p. 22). The study found that the nasal papilla was 'an adaptation to the hydrodynamic situation, including boundary layer effects of the longirostrate fish', but no further details were given.

The current study forms part of a programme to understand the hydrodynamics of olfaction in fishes, an important but largely unexplored area (Cox, 2008; Abel et al., 2010; Holmes et al., 2011; Howard et al., 2013; Agbesi et al., 2016).

2. Materials and methods

2.1 Specimens

Specimens were from the Natural History Museum, London, UK. The catalogue numbers and total lengths (Fig. 1, *TL*) of the 11 specimens of garpike (*Belone belone*) that we examined are BMNH 1939.6.27.3 (one specimen, *TL* 61 cm), BMNH 1981.2.2.3-4 (two specimens, *TL* 43 and 45 cm), BMNH 1995.8.22.5 (one specimen, *TL* 42 cm), and BMNH 2005.4.27.24-30 (seven specimens, e.g. Fig. 2A; *TL* 53 - 76 cm). All 11 specimens have well-preserved nasal regions (Fig. 3; cf. Theisen et al., 1980, Fig. 1c - anterior is to the top left of the latter figure, posterior to the bottom right). Specimens BMNH 2005.4.27.24-30 comprise the head only (up to and including the pectoral fins; Fig. 1, PF); the other specimens are intact. The total lengths of BMNH 2005.4.27.24-30 are based on Wheeler (1969, p. 236) and a comparison with 20 full length garpike specimens (BMNH 1987.3.27.1-27). We used BMNH 2015.4.9.1 (one specimen), which has a pair of poorly preserved nasal regions but almost intact jaws (only the tip of the lower jaw is broken; Fig. 2B, arrow), as a photographic reference for sculpting (Section 2.2.3), and a specimen of another belonid, *Strongylura marina*, BMNH 1939.7.10.14 (*TL* 55 cm), for the same process. All specimens are stored in 70 % industrial methylated spirits, 30 % distilled water.

2.2 Construction of plastic models of the garpike's head

2.2.1 Overview

We constructed three life-like models of a garpike's head for flow visualisation: Model 1 (derived from BMNH 2005.4.27.24); Model 2 (derived from BMNH 2005.4.27.25); and Model 3 (derived from BMNH 2005.4.27.30). We chose these particular specimens for model building because: a) they had relatively large, well-preserved nasal regions; b) they showed good variety in the morphology of their papillae (Fig. 3; Section 3.1); and c) they were amenable to X-ray scanning (all but one of the other garpike specimens with well-preserved nasal regions had bent bodies, making their heads awkward to scan). To construct the models, we X-ray scanned, using micro-computed tomography (micro-CT), the preserved specimen, converted the X-ray scan into a stereolithography (STL) model, and then 3D printed the STL model. The bent or broken jaws of the specimens were repaired in the STL models

using sculpting software. Sculpting was aided by referring to photographs of garpike with intact or mostly intact jaws. In addition, we used an STL model of the head of *Strongylura marina* to sculpt the jaws of Model 2, which were largely missing from the X-ray scan of BMNH 2005.4.27.25; the jaws of the specimen of *Strongylura marina*, on the other hand, are completely intact and were fully captured when this specimen was X-ray scanned. The models were 3D printed from black plastic in order to give good contrast with the green dye used for flow visualisation. The models were twice life-size to enable us to match the flow speed in our experiments to the estimated swimming speed of the garpike. To reduce any adverse fluid dynamic effects resulting from the lack of a body (Abel et al., 2010, pp. 472-473), we artificially extended the head (Fig. 4B and E, Ex).

2.2.2 Micro-CT

Micro-CT of the heads of the specimens of garpike (BMNH 2005.4.27.24, BMNH 2005.4.27.25 and BMNH 2005.4.27.30) and *Strongylura marina* was performed using either an HMXST 225 or an MCT225 CT system (Nikon Metrology, Tring, UK). Scans were performed in air, with the long axis of each head vertical. The X-ray beam was generated from a tungsten target. The accelerating voltage and current were 90 kV and 324 μA (BMNH 2005.4.27.24 and 30), 180 kV and 115 μA (BMNH 2005.4.27.25), and 180 kV and 200 μA (*Strongylura marina*). A total of 3,142 projections were collected in a single 360° rotation at 0.11458° intervals for BMNH 2005.4.27.25 and *Strongylura marina*, and 3,141 projections at 0.11461° intervals for BMNH 2005.4.27.24 and BMNH 2005.4.27.30. The projections were transformed into a 3D matrix using CT-Pro (Nikon Metrology). Voxel sizes were 30 μm x 30 μm x 30 μm (garpike) and 97 μm x 97 μm x 97 μm (*Strongylura marina*). Pectoral fins (Fig. 1, PF) were not included in the scans. To create the STL models, each scan was converted into a set of DICOM or TIFF images (Fig. 5) using VGStudio MAX (Volume Graphics GmbH, Heidelberg, Germany).

2.2.3 STL models

STL models were created with the image processing software ScanIP (Versions 5 or 7, Simpleware, Exeter, UK) and the sculpting software ZBrush (Version 4.7, Pixologic, California, USA) as follows. DICOM and TIFF images from the X-ray

scans were imported into ScanIP and segmented (Soille, 1999) with the Threshold tool, generating 'masks' of the heads (Fig. 5B, Ma). The size of each mask was increased by a factor of two (leading to 2x life-sized plastic models) with the Rescale tool. The garpike masks were extended 5 cm caudally with the Pad and Paint tools (Fig. 4B, Ex). In the flow visualisation experiments, the posterior edges of the models were therefore 6 – 9 characteristic dimensions (the height of the nasal cavity; Fig. 3E, *L*) downstream from the posterior edges of the nasal cavities, a distance we considered sufficient to render upstream effects negligible. A hole was created in the back of the extension with the Paint tool, to allow an aluminium peg (Fig. 4E, Pe) to be fitted to each plastic model. The mouth and gill regions of the garpike masks were filled with the Floodfill and Paint tools (cf. Fig. 5A and B) to reduce the file size. The Floodfill tool was also used to remove the base of the jaws of the mask corresponding to Model 2. Surface models of the masks were created with 10 iterations of post-smoothing and 20 % reduction in triangles. The surface models were exported as binary STL models, imported into ZBrush, and converted into meshes. The bent tips of the jaws of the meshes of Models 1 and 3 were straightened by severing each tip with the Slice Curve tool, rotating the detached tip with the Transpose tool, and then reattaching the tip with the Dynamesh tool to create a single mesh. The joint was sculpted with the Move, Clay, Dam Standard and Smooth tools, giving a seamless progression from the tip to the rest of the jaws. Alignment of the tip, and subsequent sculpting, was aided by overlaying semi-transparent photographs of BMNH 2015.4.9.1 (Fig. 2B) and other garpike with intact jaws. The missing jaws of the mesh of Model 2 were restored using the jaws of the *Strongylura marina* mesh, which were severed, attached to the mesh of Model 2, and then sculpted to give a smooth joint (Fig. 4B, black arrow) using methodology similar to that used to straighten the tips of the meshes of Models 1 and 3. The gap between the jaws of specimen BMNH 2005.4.27.25 (Fig. 2A, Mo) was filled during the sculpting process (Fig. 4B, white arrow). The eyes of the mesh of Model 2 were sculpted separately, each from the mesh of a sphere. The file size of the meshes of Models 1-3 was reduced (without affecting surface detail) using the Decimation Master tool, and the meshes exported as STL models. These models were then used to 3D print the plastic models.

2.2.4 Plastic models

The plastic models were 3D printed from the corresponding STL models according to the methodology of Abel et al. (2010, p. 468). All three models were printed in black plastic (ABS-M30 or ABA, Stratasys, Eden Prairie, USA). The resultant models comprised layers 178 μm thick, discernible by eye, with the layers perpendicular to the long axis of the heads. An aluminium peg was inserted into the back of each model (Fig. 4E, Pe).

2.3 Flow visualisation

We visualised flow in the nasal regions of the plastic models in a closed-circuit, free-surface, continuous-flow flume in the Department of Mechanical Engineering at the University of Bath. The working section of the flume is (L x W x H) 152 cm x 38 cm x 51 cm. Full details of the flume are given in Wang et al. (2007, p. 1879) and Table A2 of Abel et al. (2010). We operated the flume at free-stream flow speeds of 5, 10, 15, 20 and 24 cm s^{-1}. Given that the models were 2x life-size, these speeds would, according to the principle of dynamic similarity (Shapiro, 1961, pp. 106-107; Vogel, 1994, p. 102), correspond to swimming speeds of 10 – 48 cm s^{-1}.

The models were suspended in the flume using the rig described in Abel et al. (2010, p. 469), and positioned such that they were central (± 2 cm) width-wise to the working section of the flume. The aluminium peg (Fig. 4E, Pe) allowed each model to be positioned with the sides of the head parallel either to the sides of the flume, or to its floor. The maximum transverse cross-sectional area of the models was 24 cm^2, less than 5% of the working cross-sectional area of the flume. Therefore, based on standard corrections (Barlow et al., 1999, p. 361), the effect on flow in the vicinity of the models from the walls of the flume was deemed negligible. We investigated olfactory flow at angles of attack (Fig. 4B, An; Vogel, 1994, Fig. 11.1) of 0° ± 10°, corresponding to either the garpike ascending (+10°), descending (-10°), or swimming horizontally (0°). Separately, we investigated the effect of yaw (Fig. 4D, Ya; Sutton, 1949, Fig. 22) on olfactory flow at angles of ± 10°. The choice of yaw angles was based on Liao (2002, Fig. 8C).

Models were illuminated with an open face tungsten lamp. The green dye used to visualise olfactory flow was rhodamine 6G (0.4 mM). The dye solution was neutrally

buoyant, to give an accurate portrayal of flow (Lim, 2000, p. 44). Black card was placed behind the models to aid dye visualisation. The dye solution was introduced from a reservoir under constant pressure using stainless steel tubing (internal diameter = 1.3 mm, external diameter = 2 mm). The horizontal section of this tubing, from which the dye was released, was 23 to 30 cm from the floor of the flume. When the flow speed in the flume was 5 cm s^{-1}, dye emerged from the tubing as a thin filament; at higher speeds, dye emerged as a more dispersed stream. Dye was directed at either the tip or the base of the jaws. The distance from the tubing's outlet to the point of impingement on the model varied from 2 to 12 cm. The temperature of the water in the flume varied from 12 to 16 °C, and never by more than 1 °C in one day. Flow visualisation experiments were recorded on either Panasonic HC-V500 or Sony HDV Handycam HDR-FX7 digital camcorders. Footage was analysed with VLC media player (VideoLAN).

2.4 Reynolds numbers in the nasal region

Reynolds numbers (*Re*) of flow in the nasal regions of a) the 11 garpike specimens with well-preserved nasal regions (Section 2.1) and b) the plastic models of the garpike heads were calculated using the equation (Chance and Craig, 1986, p. 1296; Vogel, 1994, p. 85):

$$Re = \frac{UL}{\nu} \qquad \text{Equation 1}$$

where U is the speed of the fluid, L is the characteristic dimension of the object, and ν is the kinematic viscosity of the fluid. In the case of the 11 garpike specimens with well-preserved nasal regions, U is the speed at which these specimens are likely to have swum and L is the height of their nasal cavities (3.5 – 8.5 mm; Fig. 3E). The speeds at which adult garpike swim have not been reported in the scientific literature. However, the related *Strongylura marina* swims steadily at speeds of 0.25 – 2.0 *TL* s^{-1} (Liao, 2002). Given that the overall morphology of *Strongylura marina* is similar to that of the garpike - cf. Fig. 1 with Fig. 1 of Liao (2002) - garpike are likely to swim steadily at similar speeds. Therefore, assuming *TL*s of 42 - 76 cm (Section 2.1), we estimated that the garpike specimens with well-preserved nasal regions swam at 11 – 152 cm s^{-1}. In the case of the plastic models, U is the free-stream flow speed in the

flume (5 - 24 cm s^{-1}), and *L* is the height of the nasal cavity (11 – 16 mm). The kinematic viscosity of sea water between 5 and 25 °C (the average surface temperatures of the waters around Europe [Neumann and Pierson, 1966, Figs. 14.7-8], where garpike are found [Wheeler, 1969, p. 237]), is 1.0 - 1.6 x 10^{-6} m^2 s^{-1}, and water between 12 and 16 °C (the temperature in the flume) is 1.1 - 1.2 x 10^{-6} m^2 s^{-1} (calculated from Denny, 1993, Table 4.3 and Figs. 4.3 and 5.3). Reynolds numbers are given to one significant figure.

2.5 Thickness of boundary layer in the nasal region

The thickness of the boundary layer (δ) at the point where the papilla protrudes from the nasal cavities of a) the 11 garpike specimens with well-preserved nasal regions (Section 2.1) and b) the plastic models was estimated using the equation (Vogel, 1994, p. 158):

$$\delta = 5\sqrt{\frac{x\nu}{U}} \qquad \text{Equation 2}$$

where in this case *x* is the distance from the posterior edge of the needle-like section of the jaws to where the papilla protrudes (Fig. 4B, Ne) in the specimens with well-preserved nasal regions (25 - 48 mm) or the plastic models (63 -75 mm; Fig. 4B), ν is the kinematic viscosity of sea water or the water in the flume, and *U* is either the speed at which the garpike specimens are likely to have swum steadily *in vivo*, or the flow speed in the flume (Section 2.4). We measured *x* from the posterior edge of the needle-like section of the jaws rather than from the tip of the jaws because the influence of the needle-like section of the jaws (small transverse cross-sectional area) on flow will be small relative to the region caudal to this section (large transverse cross-sectional area). Equation 2 assumes that flow is laminar and that garpike are flat plates. Thus, the estimates of boundary layer thicknesses, which are given to one significant figure, are crude. The papillae of the specimens with well-preserved nasal regions may protrude up to 1 mm from the surface of the head.

3. Results

3.1 Nasal morphology

Inspection of 11 garpike specimens with well-preserved nasal regions revealed variation in nasal morphology within the same specimen and between specimens (Fig. 3, which shows the nasal regions of six of these specimens). The papilla (Fig. 3B, dashed curve) was the most variable nasal feature, appearing in two principal forms that we refer to as type I and type II. Both types occurred with equal frequency. The type I papilla (e.g. Fig. 3A), situated in the centre of the nasal cavity, had a smooth, unfolded, convex anterior surface (Fig. 3D, dashed curve) and a generally amorphous posterior surface (Fig. 3A, dashed curve) that was ridged in one instance (Fig. 3J, Rd). The angle at which the anterior surface was inclined varied considerably (cf. Fig. 3B and E). In addition, this surface could be either perpendicular to the head (Fig. 3G), or inclined forwards (Fig. 3J). The lateral edge of the type I papilla could be thick (Fig. 3J) or thin (Fig. 3L). The type II papilla consisted of a flap of thin tissue folded caudally (Fig. 3C). Like the type I papilla, the anterior surface of the type II papilla was smooth (Fig. 3F, dashed curve) and the posterior surface amorphous. The type II papilla was usually located caudally (Fig. 3C), but could be located more centrally (Fig. 3K). In addition, the type II papilla was aligned close to the dorsoventral axis. Both types of papilla could either protrude or not protrude from the surface of the head with approximately equal likelihood.

Other variable features in the nasal region were: a) the presence or absence of a depression on the dorsal anterior edge of the nasal cavity (Fig. 6A, Dp); b) the presence or absence of a ridge on the ventral anterior edge of the nasal cavity (Fig. 6A, Ri); c) the shape of the nasal cavity, which could be regular (Fig. 3A) or extended dorsoventrally (Fig. 3F); d) the depth of the nasal cavity (usually deep); and e) the ventral apex (Fig. 3B, VA), which could be elongated in a variety of ways, e.g. long and narrow (Fig. 3B) or short and broad (Fig. 3K).

All the specimens we examined had a degree of asymmetry in their nasal regions, ranging from mild (e.g. the inclination of the papilla: Fig. 3A and D) to moderate (e.g. the inclination of the papilla *and* whether or not the papilla protruded from the surface of the head; Fig. 3B and E) to strong (e.g. two types of papilla; Fig. 3I and L).

Close inspection of the ventral region of the nasal cavity revealed a small aperture located behind the posterior edge (Fig. 6, yellow ellipses and Fig. 7, Ap). The aperture, which was observed in all of the specimens where we had unobstructed views of the ventral region, could be linked to the ventral apex by a narrow external channel (Fig. 7, Ch, and dashed lines). Semi-transparent versions of Models 1-3 showed that the aperture was linked to a system of internal channels (Fig. 6B, black outline) which in turn were linked to pores on the external surface of the models (e.g. Fig. 6A, circles).

3.2 Models

The plastic models encompassed some of the variable morphology of the garpike's nasal region. Importantly, the models contained both principal forms of the papilla, i.e. type I and type II. Thus, Models 1 and 2 contained the type I papilla; Model 3 contained the type II papilla (Fig. 3 and 4). The models' nasal cavities showed variety in the triangular shape (regular or dorsoventrally extended; parental specimens: Fig. 3A and F, respectively) and in the form of the ventral apex (long and narrow or short and wide; parental specimens: Fig. 3C and A, respectively), but not in depth (all were deep). The asymmetry in the models' nasal regions was mild to moderate: Model 1's nasal regions were mildly asymmetric in the angle of attack of the type I papilla (Fig. 3A and D); Model 2's nasal regions were asymmetric in the angle of attack of the type I papilla (Fig. 3B and E) and the protrusion of the papillae from the surface of the head (the left papilla protruded but the right did not); Model 3's nasal regions were mildly asymmetric in the shape of the nasal cavity (Fig. 3C and F). Thus, overall, Model 1 and 3's nasal regions were mildly asymmetric and Model 2's nasal regions were moderately asymmetric.

Comparison with the parental specimens suggested that the models were anatomically accurate in most respects, particularly in the nasal region. The two ventral apices of Model 3 were, however, less pronounced than in the parental specimen. In addition, we filled the gap in Model 2's mouth (Fig. 2A, Mo) when we reconstructed its jaws (Fig. 4B, white arrow). This gap was not filled in Models 1 and 3, however (Fig. 4A and C). In Model 2 we also replaced the sunken eyes of the parental specimen with shapes that we considered to be more like the eyes *in vivo*. Additionally, we filled the small aperture in the ventral region of each nasal cavity in all three models.

Note that the shortness of the jaws of Model 3 (Fig. 4C, asterisk) is not an artefact – the jaws of the parental specimen are intact and faithfully reproduced in this model (although the bent tip of the specimen's lower jaw has been straightened).

3.3 Flow visualisation

At all free-stream flow speeds employed (a range equivalent to swimming speeds of 10 – 48 cm s^{-1} and Reynolds numbers of 700 – 2,000), and at all model orientations (angle of attack: 0 ± 10°; yaw: 0 ± 10°; Fig. 4B and D), dye entered the nasal cavity and circulated within it (Fig. 8; Videos 1-12). At the lowest flow speed employed, dye passed over the anterior section of the head as a film (Fig. 8A, Fm), or in diffuse waves (Fig. 8E, Wa), and reached the nasal region whether directed at the dorsal or ventral regions of the jaws (Fig. 8A and B). Dye could also reach the nasal region from the mouth (Fig. 8C; Video 3). The form in which dye passed over the anterior section of the head (film or waves) did not affect the pattern of flow within the nasal cavity. Movement of dye in the nasal cavity was noticeably slower than movement of dye in the free-stream (Videos 5, 6 and 12), although the rapidity of circulation increased with increasing flow speed (e.g. Video 2). Dye was thoroughly dispersed in the nasal cavity at higher flow speeds (Videos 2, 7 and 9-11), but not always at lower speeds (Fig. 8C, D and E). At the lowest flow speed employed, dye could remain in the nasal cavity up to at least a minute after its supply had been switched off.

Flow in the nasal region was greatly influenced by whether or not the papilla protruded from the surface of the head (Fig. 2A, inset, yellow arrow). In those model nasal regions that contained a *protruding* papilla, dye entered the nasal cavities primarily as a result of it striking the papilla, irrespective of the papillar type (I or II). Circulation of dye in these nasal cavities occurred as the result of it moving around the edges of the papilla (Fig. 9B, D and E; Videos 1-3 and 8-12). Dye moving around the dorsal edge of the papilla entered either the recess of the nasal cavity (Fig. 9B, D and E, red arrows), occupying the recess fully, or the posterior region (Fig. 9B, D and E, upper yellow arrows). At certain non-zero angles of attack and yaw, and higher flow speeds, dye moved around the ventral edge of the papilla to occupy the posterior region of the nasal cavity (Fig. 9B, D and E, lower yellow arrows). On striking a protruding papilla, dye appeared as a tube, suggestive of a vortex (Fig. 8A-C, E and F;

Videos 1-3 and 12). Waves of dye within this tube-like structure moved along the surface of the nasal cavity in the opposite direction to free-stream flow. The tube-like structure occupied the recess of the nasal cavity, and the section between the papilla and the anterior edge of the nasal cavity (Fig. 8A-C, E and F). In a model nasal cavity with the type I papilla, the tube-like structure extended to the region posterior to the papilla (Fig. 8A-C). Dye circulated posterior to the type I papilla in a fashion suggestive of one or more vortices (e.g. Fig. 9G and H; Videos 1-4, 9 and 10). In a model nasal cavity with the type II papilla, dye circulated in the region posterior to the papilla as slowly moving waves (Video 12) or, at higher speeds, in more agitated structures (Video 11). Circulation behind the type II papilla at lower flow speeds required specifically that a dye filament impinged on the dorsal edge of the papilla (Fig. 8F); circulation behind the type II papilla at lower flow speeds was not observed when dye entering the nasal cavity was more diffuse (Fig. 8E). Dye behaved similarly in the two nasal regions of Model 3, which each contained a type II papilla. At certain non-zero angles of attack and yaw, dye entered a model nasal region with a protruding papilla by striking the back wall of the nasal cavity (Fig. 9B and E, dashed lines) rather than the papilla, whereupon it circulated in the region posterior to the papilla, but not in the remainder of the nasal cavity (e.g. Fig. 8D; Video 4). Circulation of dye in these instances occurred in a vortex-like structure (Fig. 8D; Video 4), or in waves.

Dye entered the left nasal cavity of Model 2, which contained a *non-protruding* type I papilla, when deflected by its posterior wall (Fig. 9C, dashed line), or the posterior apex (Fig. 9C, PA; see also Videos 5-7 for the ensuing observations on flow in this nasal cavity). Although in dorsal views of Model 2 we observed dye striking the left nasal papilla, it did not seem to be deflected into the nasal cavity by this papilla. Circulation of dye in the left nasal cavity of Model 2 occurred either around the papilla or over it. Circulation of dye around the papilla occurred when dye striking the posterior wall moved into (Fig. 9C, upper yellow arrow) and through the dorsal region of the nasal cavity in a direction *counter* to free-stream flow (Fig. 9C, green arrow) and then passed around the anterior apex (Fig. 9C, AA) and into the anterior region (Fig. 9C, red arrow). Dye also moved through the posterior region (Fig. 9C, middle yellow arrow) into the ventral apex (Fig. 9C, VA), where it then met flow that had passed through the anterior region (Fig. 9C, red and lower yellow arrows). Circulation of dye over the papilla occurred when dye striking the posterior wall of the nasal

cavity moved in an anterior direction, in waves that almost completely covered the papilla (Fig. 9C, light blue arrow) - the anterior ridge of the papilla (Fig. 9C, dashed yellow line) prevented complete circulation over the papilla. At higher flow speeds, dye occasionally appeared to move in a sinusoidal fashion through the posterior region, suggestive of a vortex (Fig. 9F, yellow arrow; Video 7). Some vortex-like behaviour was also observed in the anterior apex at these higher flow speeds (Fig. 9F, green arrow).

Dye exited a nasal cavity via the dorsal edge, the posterior edge, or the ventral apex (Fig. 9B-E, white arrows 1-3, respectively). Excurrent dye passed either over the head, or around or over the eye (Figs. 8 and 9A; Videos 1-12). We did not notice any difference in the behaviour of dye flowing from the nasal cavities of all three models, suggesting that excurrent flow was similar whether the eyes were protruding or sunken, and that Model 3's less pronounced ventral apices did not adversely affect this flow.

4. Discussion

Our first objective was to show that olfactory flow in the garpike (i.e. bulk movement of water in its nasal region) can be generated by swimming. We achieved this (Fig. 8; Videos 1-12) by moving water over static, life-like, plastic models of the adult garpike's head under physiologically relevant conditions (Reynolds numbers 700 – 2,000; angle of attack/yaw 0 ± 10°). Motion-driven olfactory flow occurred despite morphological variation in the garpike's nasal region, variation that resulted in a degree of asymmetry (mild to strong) between the paired nasal regions of the same specimen (Fig. 3).

Our second objective was to determine how the unusual features of the garpike's nasal region (nasal cavity, papilla, ventral apex: Fig. 3) influence olfactory flow and the likely effect of these influences on odorant sampling in the garpike. The nasal cavity influences olfactory flow in three ways. First, its posterior wall and posterior apex deflect flow into the cavity proper, trapping a portion of the oncoming flow (Fig. 9B, C and E, dashed white lines). Second, it acts as a site for circulating water, facilitating diffusive odorant transport to the olfactory epithelium by maintaining a

concentration gradient between it and the aqueous phase (Cox, 2008, p. 581). Third, the nasal cavity increases the residence time of fluid in the nasal region, increasing the time available for diffusion of odorant molecules to the olfactory epithelium (LaBarbera and Vogel, 1982, p. 56).

The papilla, if it protrudes from the surface of the head, may influence olfactory flow by deflecting external flow into the nasal cavity, causing circulation of water within it (Fig. 9B, D and E), and therefore dispersal of odorant molecules over the olfactory epithelium (Holmes et al., 2011, p. 1046). Both type I and type II papillae cause circulation within the anterior and dorsal regions of the nasal cavity via similar types of flow structure (Fig. 8A and F, Vo). Although water circulated effectively posterior to both types of papilla (Fig. 9B, D and E), the more centrally located type I papilla permits a greater variety of flow structures in this region. The inclination of the type I papilla, together possibly with the shape of the nasal cavity, may influence the nature of these flow structures. When the type I papilla did not protrude from the surface of the head, circulation occurred as a result of flow striking the posterior wall of the nasal cavity, and in the opposite direction to free-stream flow (compare Fig. 9C with Fig. 9B, D and E). The texture (smooth) and shape (convex, or folded caudally) of the anterior surface of both types of papilla are likely to reduce drag; the irregular posterior surface of the papilla may increase the sensory surface area, facilitating odorant transport to the olfactory epithelium (Schmidt-Nielsen, 1997, p. 586).

Irrespective of its shape (long and narrow or short and wide), the ventral apex of the nasal cavity acts as a conduit for flow leaving the nasal cavity, encouraging circulation within it, although flow can also leave by passing over the dorsal and posterior edges (Fig. 9).

Unexpectedly, we found that the dorsal and ventral regions at the base of the jaws (Fig. 2A, white disks; Fig. 9A), and the mouth (Figs. 8C and 9A), also influenced olfactory flow. The dorsal region at the base of the jaws, which is arched (Fig. 2B, Ar), is supported by the premaxilla (Pm, Fig. 2C); the ventral region is supported by the dentary (Fig. 2C, De; Gregory, 1933, Fig. 99). Both regions disperse and retard flow prior to it reaching the garpike's nasal cavity, and together ensure that water is sampled over a relatively large cross-sectional area. The mouth, at least in our plastic

models, may serve as a source of olfactory flow, capturing and subsequently releasing water over the nasal region (Figs. 8C and 9A), causing a delay in the sampling process. The gap in the mouth where the dye collected in our flow visualisation experiments was almost always present in the specimens we examined (Fig. 2A; but see also Fig. 2B, where it is less pronounced). The mouth's influence on olfactory flow could, however, be countered *in vivo* by the action of the respiratory pump. Three further anatomical features that are likely to have an influence on olfactory flow, but which we did not investigate, are the depth of the nasal cavity, and the ridge and depression anterior to the nasal cavity (Fig. 6A). Another feature, a small aperture situated in the ventral region of the nasal cavity, is unlikely to significantly affect olfactory flow, because it appears to be part of the garpike's lateral line system (Parin and Astakhov, 1982) and, if so, it will be filled with a viscous fluid *in vivo* (Kasumyan, 2003, p. S184).

We estimate the thickness of the boundary layer in the garpike's nasal region to be 0.6 - 4 mm. Consequently, the papilla, which in some specimens can protrude by up to 1 mm from the surface of the head, may extend into the free-stream, particularly (Equation 2, Section 2.5) at faster swimming speeds, or at higher temperatures (the kinematic viscosity of sea water decreases with increasing temperature). Odorant transport to the olfactory epithelium lining the papilla is more likely to be favoured when the papilla extends through the boundary layer and into the free-stream because boundary layers act as barriers to odorant transport (Vogel, 1994, pp. 161-162; Cox, 2008, pp. 578-579). These considerations of the papilla/boundary layer interaction may have been what Zeiske and Hansen (2005, p. 22) were referring to when they stated that the papilla is 'an adaptation to the hydrodynamic situation, including boundary layer effects of the longirostrate fish'.

We have remarked previously that Reynolds numbers in the nasal region of the swimming garpike (200 – 10,000) are favourable for vortex formation (Cox, 2008, p. 587). Vortices (Lugt, 1983, pp. 18-19) could help disperse odorant molecules over the olfactory epithelium and also enhance their transport to it, in the latter case by producing steep velocity gradients (Vogel, 1994, pp. 196-197, p. 212 and p. 356); beating non-sensory cilia in the olfactory organs of some fishes are also likely to produce steep velocity gradients (Cox, 2008, pp. 581-582). We observed several flow

structures suggestive of vortices. The clearest of these was the tube-like structures that formed around protruding papillae at lower free-stream flow speeds (Fig. 8A-C, E and F; Videos 1-3 and 12), structures reminiscent of a horseshoe vortex (Lugt, 1983, pp. 85-86; Vogel, 1994, Fig. 10.8). Horseshoe vortices form around objects that protrude into the boundary layer (Lugt, 1983, p. 85), as five of the model papillae did in our experiments (the five papillae protrude by 0.5 - 1 mm from the surface of the model heads; the thickness of the boundary layer was 3 - 7 mm). The direction that fluid moved within the tube-like structures was consistent with that expected for a horseshoe vortex (Lugt, 1983, Fig. 5.65; Vogel, 1994, Fig. 10.9). We also observed various vortex-like structures between type I papillae and the posterior wall of the nasal cavity (Fig. 9F-H; Videos 1-4, 7, 9 and 10), including one that resembled a pair of coupled vortices (Fig. 9G, yellow arrows, and Video 9; Vogel, 1994, p. 210). Although we did not investigate their influence in any systematic way, we suspect that the papilla's inclination, together possibly with the shape of the nasal cavity, influenced the nature of these vortex-like structures. Another vortex-like structure was observed in the anterior apex of the nasal cavity (Fig. 9F and G, green arrows). This particular flow structure was reminiscent of a vortex induced at a sharp corner (Vogel, 1994, Fig. 10.6b), which of course the anterior apex of the nasal cavity is (Fig. 3B, AA). Vortex-like structures were recently observed in the nasal region of a model guitarfish, where they may encourage olfactory flow and reduce the cost of swimming (Agbesi et al., 2016). Their apparent presence in the garpike's nasal cavity suggests that vortex-like structures may be a not uncommon element in olfactory flow in fishes (see Cox, 2008, pp. 587-588, for other situations in which vortex-like structures may occur in the nasal regions of fishes).

To some extent the garpike's nasal region resembles a NACA submerged-duct entrance ('NACA scoop': Fig. 2 of Frick et al., 1945). NACA scoops were developed to reduce drag and pressure losses in the air-induction systems of aircraft (Mossman and Randall, 1948). Like the garpike's nasal cavity, the walls of a NACA scoop diverge in the direction of flow and possess sharp edges. Both features are a form of boundary layer control, and have the effect of reducing pressure losses: the diverging walls divert the boundary layer around the entrance of the NACA scoop, whilst the sharp edges prevent the boundary layer flowing into the NACA scoop (Mossman and Randall, 1948, pp. 6-7). A similar form of boundary layer control may be occurring in

the garpike's nasal region. It should be noted, however, that the garpike's nasal region is a cavity rather than a duct, and its purpose is to sample odorants rather than to provide a channel for fluid to flow through.

Whilst the nasal region of the garpike is unusual, it is not unique: there are other beloniforms whose nasal regions are similar (Blaue, 1884, pp. 241-247; Burne, 1909, pp. 634-635; Singh, 1977, Figs. 1-6; Yamamoto and Ueda, 1979, Fig. 1a and b; Theisen et al., 1980, p. 167; the papilla in Fig. 1b of Yamamoto and Ueda, 1979, resembles the type II papilla of the current study). These fishes include other species in the family Belonidae (needlefishes), and species belonging to the families Exocoetidae (flyingfishes), Hemiramphidae (halfbeaks, including the genus *Rhynchorhamphus*, which has a fimbriate nasal papilla; Collette, 1976, Fig. 1), and Scomberesocidae (sauries). Given the similarity of the nasal regions of these fishes to that of the garpike, we suggest that olfactory flow in these fishes is also similar. However, there are some beloniforms in which the papilla is elongated and protrudes markedly from the surface of the head (Singh, 1972, Fig. 1c; Gupta and Shrivastava, 1973, Fig. 1; Holey and Belsare, 1973, Fig. 1; Collette, 1974, Fig. 3; Anderson and Collette, 1991, Fig. 1; Greven, 2006; Zanger and Greven, 2013). Olfactory flow may be different in these particular beloniforms.

Our study was limited in two significant ways. First, we did not explore olfactory flow over the full range of Reynolds numbers in the nasal region of the swimming garpike (200 - 10,000); rather, we investigated only the lower end of this range (700 - 2,000). Olfactory flow at higher Reynolds numbers may be investigated by computational fluid dynamics (CFD), a technique that could also be used to explore further the vortex-like structures in the nasal region. Using an experimental technique such as particle image velocimetry (PIV; Gharib and Dabiri, 2000) to investigate olfactory flow at higher Reynolds numbers may not be suitable in this instance given that, for example, the sheet of laser light required for PIV cannot penetrate the nasal cavity when orientated parallel to the side of the head (HSB and JPLC, unpublished observations). Second, we did not take into account any upstream effects of the garpike's pectoral fins (absent in our models). Based on the swimming behaviour of the related *Strongylura marina*, the garpike's pectoral fins may influence olfactory flow at low (0.25 *TL* s^{-1}) to intermediate (up to 1.5 *TL* s^{-1}) swimming speeds by

oscillating or by being permanently abducted, respectively (Liao, 2002, p. 2883). This influence may be modelled by CFD, or by creating a physical model with static or moving pectoral fins.

Several lines of further enquiry are evident. One is to explore in greater detail the influence of the garpike's variable nasal morphology on olfactory flow, e.g. that of a non-protruding type II papilla, or that of a more centrally placed type II papilla (Fig. 3K), and more subtle variations such as the shape and depth of the nasal cavity. It would also be interesting to investigate the influence of the ridge and depression (Fig. 6A), and that of an artificially modified nasal cavity, e.g. one lacking a papilla. Finally, performing a flow visualisation study on another beloniform such as *Strongylura marina*, which has many nasal features similar to those of the garpike (triangular nasal cavity integrated into the surface of the head, type II papilla, ventral apex, depression; Fig. 10), is highly desirable.

5. Conclusions

Olfactory flow in the adult garpike, *Belone belone*, can be generated by swimming, and occurs despite morphological variations in the nasal region. These variations can, however, influence the *pattern* of olfactory flow. Important influences on the pattern of olfactory flow are the position of the papilla in the nasal cavity and whether or not the papilla protrudes from the surface of the head. The inclination of a type I papilla may also affect the pattern of olfactory flow in the posterior region of the nasal cavity. The nasal cavity, the papilla, the ventral apex, the base of the jaws, and the mouth may enhance odorant capture by: a) sampling water over a relatively large cross-sectional area (jaws); b) encouraging circulation of water (nasal cavity, papilla, ventral apex); c) dispersing flow over the olfactory epithelium (papilla, jaws, mouth); d) increasing the time for diffusion of odorant molecules to the olfactory epithelium (nasal cavity, jaws, mouth); and e) projecting the olfactory epithelium into the free-stream (papilla). Several different types of vortex-like structure generated within the nasal region may help disperse odorant molecules over the olfactory epithelium, and their transport to it. The type of olfactory flow we observed in the garpike may be similar in other beloniforms with exposed nasal cavities/relatively short papillae.

Acknowledgements

We thank Jim Askins for garpike specimen BMNH 2015.4.9.1, Joe Pender for the coordinates of where this specimen was caught, Laser Lines for 3D printing, Paul Frith for model assembly, Chen Chen, Joe Rodrigues, Mary Mahon, Ian Trussler, Simon Wharf, Jonathan White and Zhuoyi Ye for technical assistance, Harry Taylor and Kevin Webb for photography, Nina Martin for the X-ray image of BMNH 2015.4.9.1, Xavier Mear and Randolf Kohn for German to English translation, Bruce Collette, Oliver Crimmen, Sherrie Floyd-Cutler, Linda Humphreys, Jaclyn Pearson and Patrick Tompsett for helpful discussions, two anonymous reviewers for their valuable comments on the manuscript, and the University of Bath's Alumni Fund for financial support.

References

Abel, R.L., Maclaine, J.S., Cotton, R., Xuan, V.B., Nickels, T.B., Clark, T.H., Wang, Z., Cox, J.P.L., 2010. Functional morphology of the nasal region of a hammerhead shark. Comp. Biochem. Physiol. A 155, 464-475.

Agbesi, M.P.K., Naylor, S., Perkins, E., Borsuk, H.S., Sykes, D., Maclaine, J.S., Wang, Z., Cox, J.P.L., 2016. Complex flow in the nasal region of guitarfishes. Comp. Biochem. Physiol. A 193, 52-63.

Anderson, W.D., Collette, B.B., 1991. Revision of the freshwater viviparous halfbeaks of the genus *Hemiramphodon* (Teleostei: Hemiramphidae). Ichthyol. Explor. Freshwaters 2, 151-176.

Barlow, J.B., Rae, W.H., Pope, A., 1999. Low-speed wind tunnel testing, third ed. John Wiley & Sons, New York.

Blaue, J., 1884. Untersuchungen über den Bau der Nasenschleimhaut bei Fischen und Amphibien, namentlich über Endknospen als Endapparate des Nervus olfactorius. Arch. Anat. Physiol. 231-309.

Burne, R.H., 1909. The anatomy of the olfactory organ of teleostean fishes. Proc. Zool. Soc. Lond. 2, 610-663.

Chance, M.M., Craig, D.A., 1986. Hydrodynamics and behaviour of Simuliidae larvae (Diptera). Can. J. Zool. 64, 1295-1309.

Collette, B.B., 1974. The garfishes (Hemiramphidae) of Australia and New Zealand. Rec. Aust. Mus. 29, 11-105.

Collette, B.B., 1976. Indo-west Pacific halfbeaks (Hemiramphidae) of the genus *Rhynchorhamphus* with descriptions of two new species. Bull. Mar. Sci. 26, 72-98.

Cox, J.P.L., 2008. Hydrodynamic aspects of fish olfaction. J. Roy. Soc. Inter. 5, 575-593.

Denny, M.W., 1993. Air and Water. Princeton University Press, Princeton.

Frick, C.W., Davis, W.F., Randall, L.M., Mossman, E.A., 1945. An experimental investigation of NACA submerged duct entrances. National Advisory Committee for Aeronautics Advance Confidential Report 5120, Washington, DC.

Gharib, M., Dabiri, D., 2000. Digital particle image velocimetry. In: Smits, A.J., Lim, T.T. (Eds.), Flow Visualization. Imperial College Press, London, pp. 123-147.

Gregory, W.K., 1933. Fish skulls: a study of the evolution of natural mechanisms. Trans. Am. Philos. Soc. 23, 75-468.

Greven, H. 2006. Lebendgebärende Halbschnabelhechte. In: Greven, H., Riehl, R. (Eds.), Biologie der Aquarienfische. Tetra Verlag GmbH, Berlin-Velten, pp. 271-296.

Gupta, O.P., Shrivastava, R.K., 1973. An interesting type olfactory organ in Indian gar-fish of the family Belonidae, *Xenentodon cancila* (Ham.). Zool. Jb. Anat. Bd. 90, 450-453.

Hara, T.J., 1975. Olfaction in fish. Prog. Neurobiol. 5, 271-335.

Helfman, G.S., Collette, B.B., Facey, D.E., Bowen, B.W., 2009. The Diversity of Fishes. Wiley-Blackwell, Chichester.

Holey, D.T., Belsare, D.K., 1973. Morphology of the olfactory sac in some teleosts. Z. Mikrosk.-Anat. Forsch. 87, 463-469.

Holmes, W.M., Cotton, R., Xuan, V.B., Rygg, A.D., Craven, B.A., Abel, R.L., Slack, R., Cox, J.P.L., 2011. Three-dimensional structure of the nasal passageway of a hagfish and its implications for olfaction. Anat. Rec. 294, 1045-1056.

Howard, L.E., Holmes, W.M., Ferrando, S., Maclaine, J.S., Kelsh, R.N., Ramsey, A., Abel, R.L., Cox, J.P.L., 2013. Functional nasal morphology of chimaerid fishes. J. Morph. 274, 987-1009.

Kasumyan, A.O., 2003. The lateral line in fish. J Ichthyol. 43, Suppl. 2, S175-S213.

LaBarbera, M., Vogel S., 1982. The design of fluid transport systems in organisms. Am. Sci. 70, 54-60.

Liao, J.C., 2002. Swimming in needlefish (Belonidae): anguilliform locomotion with fins. J. Exp. Biol. 205, 2875–2884.

Lim, T.T., 2000. Dye and smoke visualization. In: Smits, A.J., Lim, T.T. (Eds.), Flow Visualization. Imperial College Press, London, pp. 43-72.

Lugt, H.J., 1983. Vortex Flow in Nature and Technology. John Wiley & Sons, New York.

Mossman, E.A., Randall, L.M., 1948. An experimental investigation of the design variables for NACA submerged duct entrances. National Advisory Committee for Aeronautics Research Memorandum A7130, Washington, DC.

Neumann, G., Pierson, W.J., 1966. Principles of Physical Oceanography. Prentice-Hall, Englewood Cliffs.

Parin, N.V., Astakhov, D.A., 1982. Studies on the acoustico-lateralis system of beloniform fishes in connection with their systematics. Copeia, 2, 276-291.

Schmidt-Nielsen, K., 1997. Animal Physiology, fifth ed. Cambridge University Press, Cambridge.

Shapiro, A.H., 1961. Shape and Flow. Heinemann, London.

Singh, C.P., 1972. A comparative study of the olfactory organ of some Indian freshwater teleostan fishes. Anat. Anz. 131, 225-233.

Singh, S.P., 1977. Functional anatomy of olfactory organs in some marine teleosts. Zool. Anz. 199, 441-444.

Soille, P., 1999. Morphological Image Analysis. Springer, Berlin.

Sutton, O.G., 1949. The Science of Flight. Penguin Books, Harmondsworth.

Theisen, B., Breucker, H., Zeiske, E., Melinkat, R. 1980. Structure and development of the olfactory organ in the garfish *Belone belone* (L.) (Teleostei, Atheriniformes). Acta Zool. 61, 161-170.

Vogel, S., 1994. Life in Moving Fluids, second ed. Princeton University Press, Princeton.

Wang, Z.-J., Jiang, P., Gursul, I., 2007. Effect of thrust-vectoring jets on delta wing aerodynamics. J. Aircr. 44, 1877-1888.

Wheeler, A. 1969. The Fishes of the British Isles and North-West Europe. Macmillan, London.

Yamamoto, M., Ueda, K., 1979. Comparative morphology of fish olfactory epithelium VIII Atheriniformes. Zool. Mag. (Zool. Soc. Jap.) 88, 155-164.

Zanger, K., Greven, H., 2013. The 'nasal barbel' of the halfbeak *Dermogenys pusilla* (Teleostei: Zenarchopteridae) – an organ with dual function. Vert. Zool. 63, 183-191.

Zeiske, E., Theisen, B., Breucker, H. 1992. Structure, development, and evolutionary aspects of the peripheral olfactory system. In: Hara, T. J. (Ed.), Fish Chemoreception. Chapman and Hall, London, pp. 13–39.

Zeiske, E., Hansen, A., 2005. Development and evolution of the olfactory organ in gnathostome fish. In: Reutter, K., Kapoor, B.G. (Eds.), Fish Chemosenses. Science Publishers, Enfield, pp. 1-29.

Figures

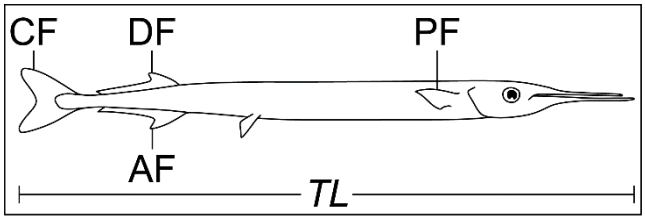

Fig. 1 Outline of garpike, *Belone belone*. Redrawn from Wheeler (1969). AF, CF, DF and PF: anal, caudal, dorsal and pectoral fins, respectively. *TL*: total length.

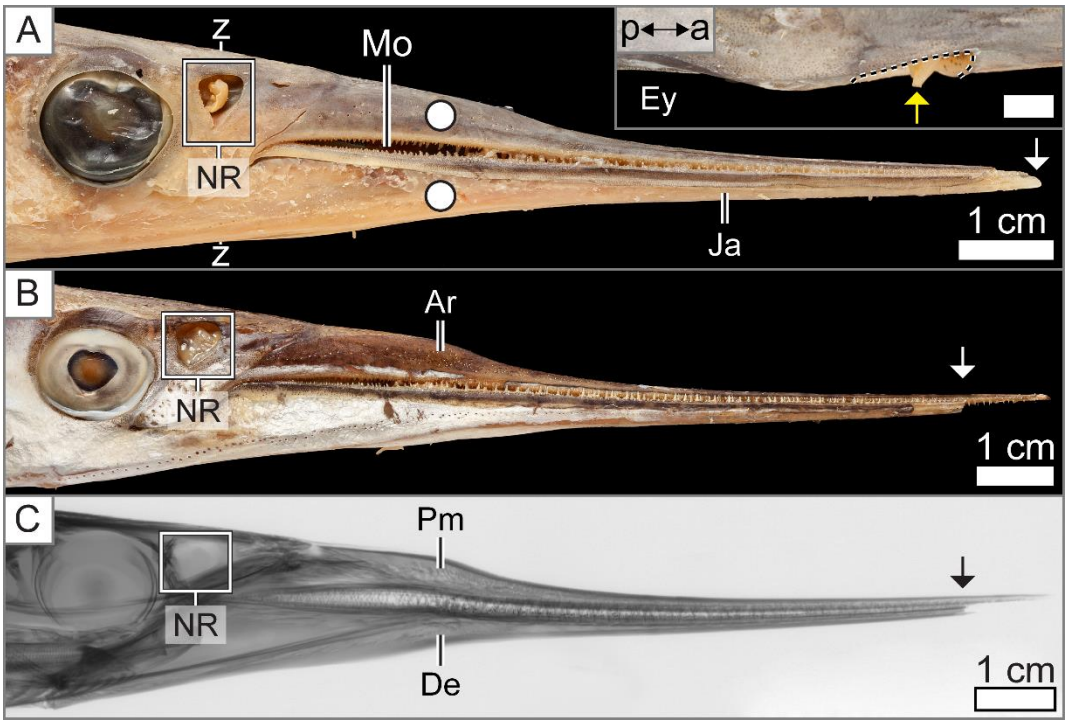

Fig. 2 Specimens of garpike, *Belone belone*, used in this study. (A) BMNH 2005.4.27.25. zz: position of cross-section shown in Fig. 5. White disks: upper and lower jaw. Inset: dorsal aspect of head, right nasal region. Dashed line: outline of nasal cavity. Yellow arrow: protruding papilla. Scale bar: 2 mm. (B) BMNH 2015.4.9.1. (C) X-ray image of BMNH 2015.4.9.1. Black and white arrows: broken jaws. a: Anterior; Ar: arch; De: dentary; Ey: eye; Ja: jaws; Mo: gap in mouth; NR: nasal region; p: posterior; Pm: premaxilla.

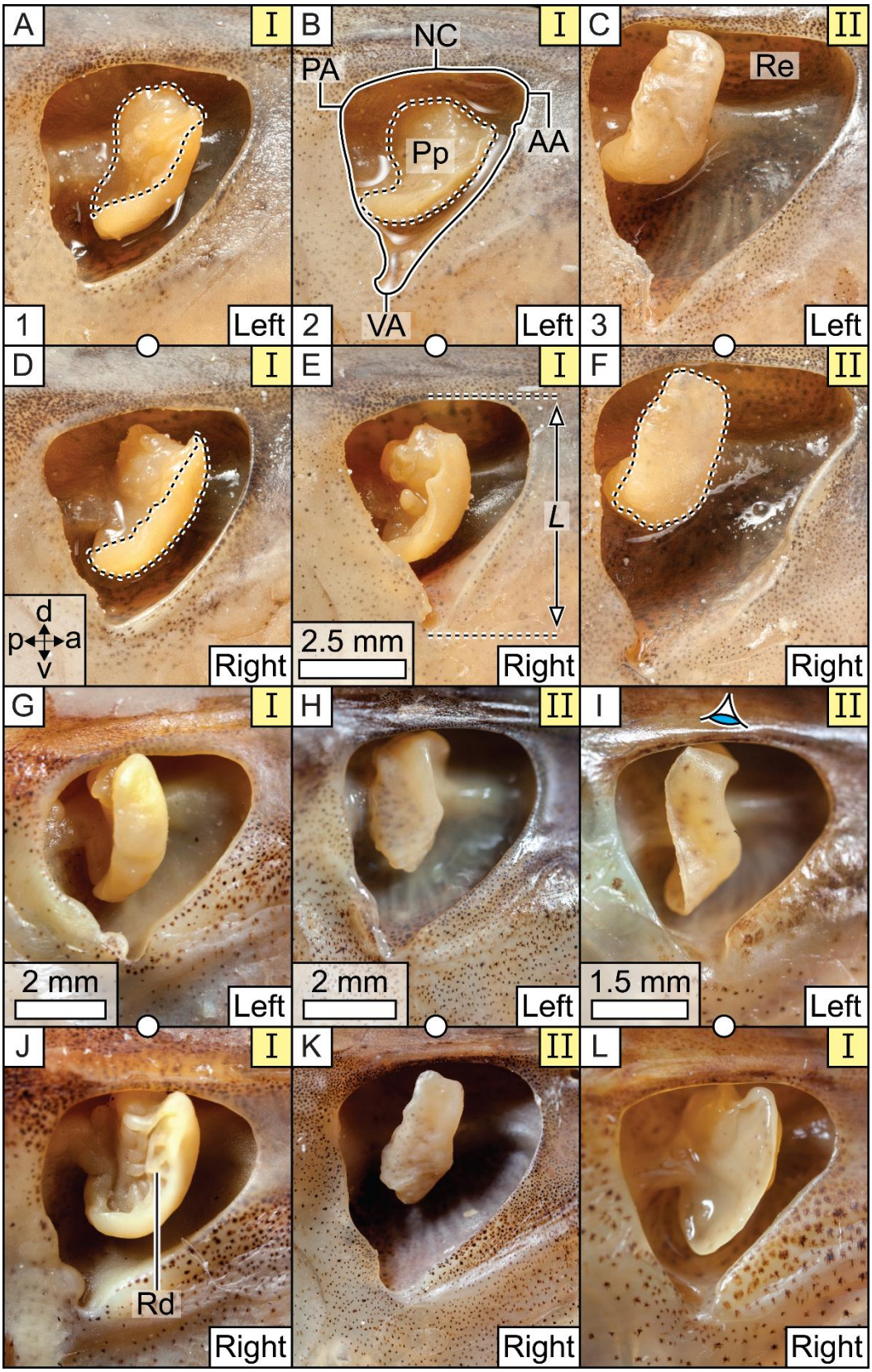
A
I
1
Left
B
NC
PA
AA
Pp
VA
I
2
Left
C
II
Re
3
Left
D
I
d
p
a
v
Right
E
I
L
2.5 mm
Right
F
II
Right
G
I
2 mm
Left
H
II
2 mm
Left
I
II
1.5 mm
Left
J
I
Rd
Right
K
II
Right
L
I
Right

Fig. 3 Paired nasal regions of six different specimens of garpike, *Belone belone*: (A) and (D): BMNH 2005.4.27.24. (B) and (E): BMNH 2005.4.27.25. (C) and (F): BMNH 2005.4.27.30. (G) and (J): BMNH 1939.6.27.3. (H) and (K): BMNH 1981.2.2.3-4. (I) and (L): BMNH 1995.8.22.5. Nasal regions from same specimen linked by white disk. Nasal region (left or right) and papillar type (I or II) designated in each panel. The number in the bottom left corner of panels (A) to (C) indicates the plastic model which contains the paired nasal regions shown. Eye in panel (I): viewpoint in Fig. 7. See main text for explanation of dashed curves. Photographs of left nasal regions inverted. Scale bar in (E) applies to panels (A) – (F). Scale bars in (G) - (I) specific to each pair of nasal regions. a: Anterior; AA: anterior apex; d: dorsal; *L*: height of nasal cavity; NC: nasal cavity (outlined); p: posterior; PA: posterior apex; Pp: papilla; Rd: papillar ridge; Re: recess; v: ventral; VA: ventral apex.

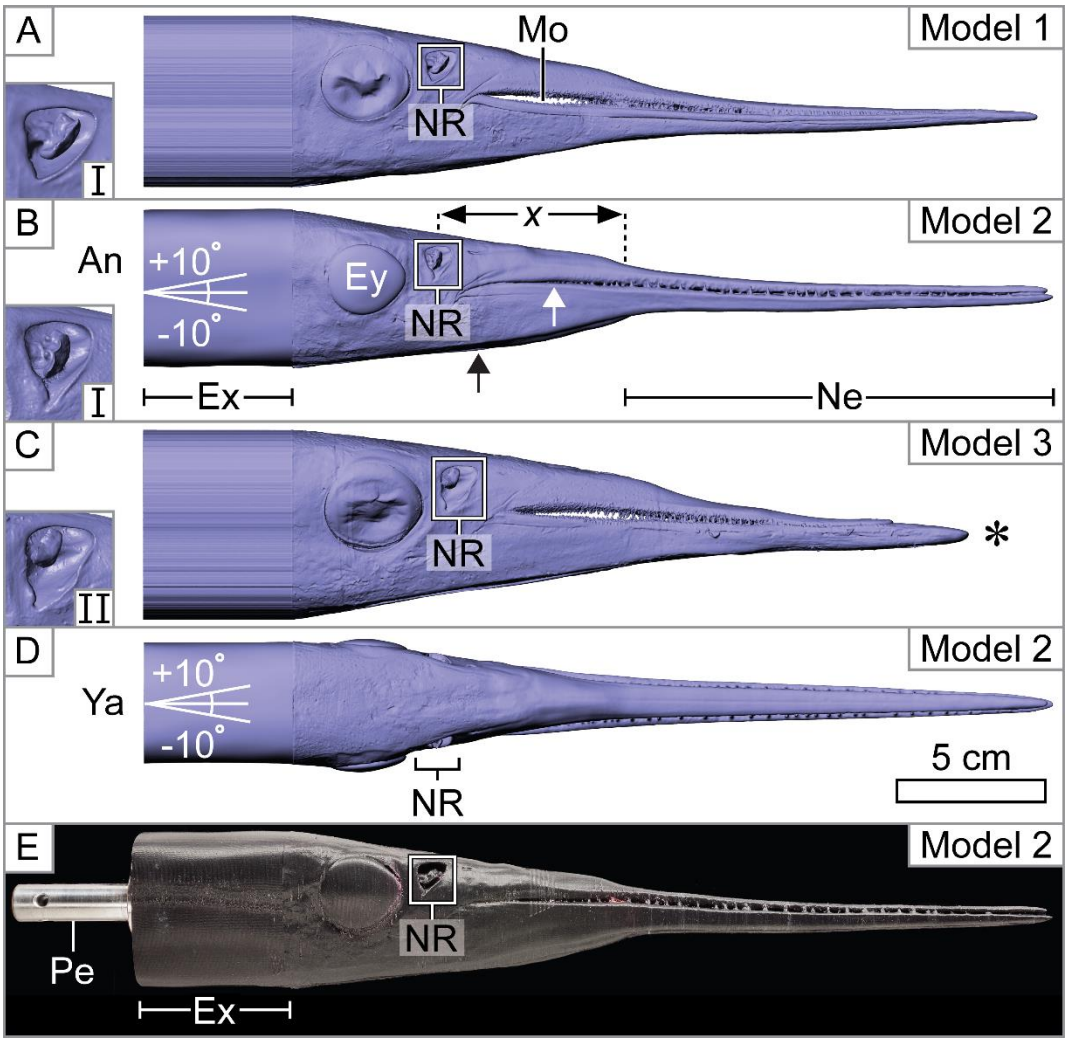

Fig. 4 Model garpike heads. (A) - (D): right side (A-C) and dorsal aspect (D) of stereolithography models. *x*: Distance used for boundary layer calculations. (E) Left side of plastic Model 2 (photograph inverted). Insets in (A) – (C) show the right nasal region and papillar type (I or II) of each model. See main text for explanation of white and black arrows and asterisk. Scale bar applies to all panels. An: angle of attack; Ex: extension; Ey: eye; Ne: needle-like section of jaws; NR: nasal region; Pe: aluminium peg; Ya: yaw.

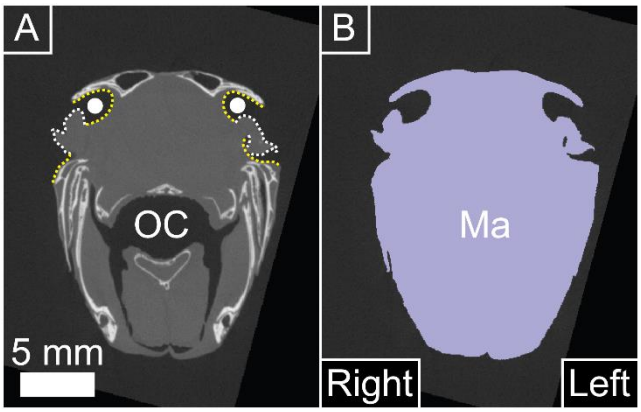

Fig. 5 X-ray micro-CT image of garpike, *Belone belone* (BMNH 2005.4.27.25). (A) Cross-section through paired nasal regions (zz in Fig. 2A). (B) Same image with mask superimposed. Yellow dotted line: nasal cavity. White dotted line: papilla. White disk: recess. Ma: mask; OC: oral cavity.

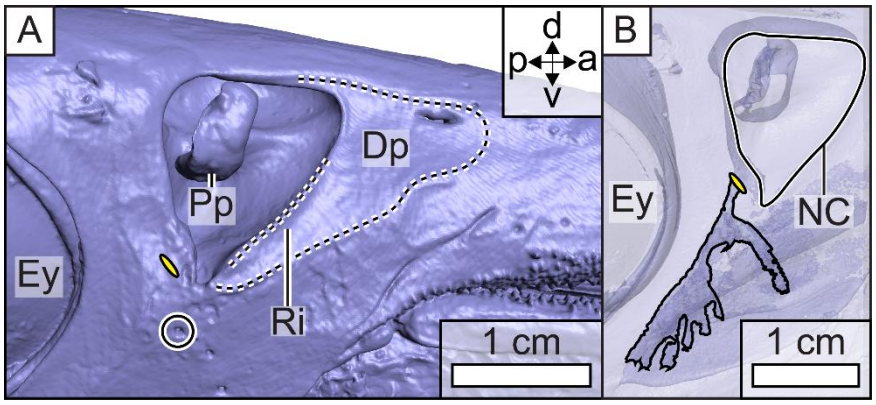

Fig. 6 Further aspects of the nasal region of the garpike, *Belone belone*. Life-sized stereolithography models of left nasal region of BMNH 2005.4.27.30 (images inverted). (A) Opaque model. (B) Semi-transparent model. Yellow ellipse: location of aperture within nasal cavity. Circle in (A): pore. Black outline in (B): internal channels to which aperture linked. a: Anterior; d: dorsal; Dp: depression; Ey: eye; p: posterior; Pp: papilla; Ri: ridge; v: ventral.

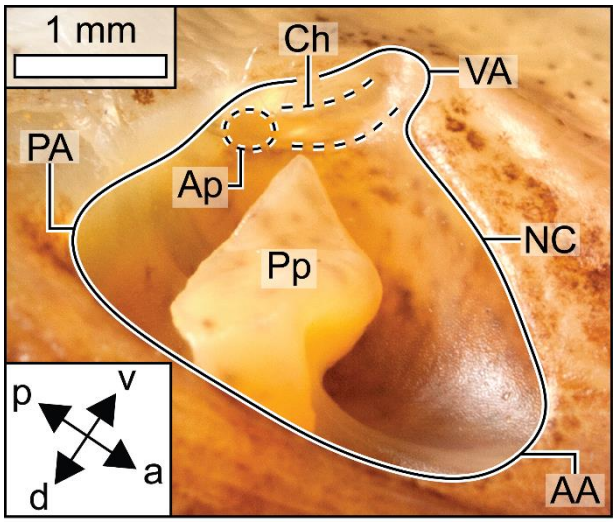

Fig. 7 Aperture in ventral region of nasal cavity of the garpike, *Belone belone*. Specimen BMNH 1995.8.22.5, left nasal region, view from above with specimen slightly tilted (eye, Fig. 3I). See main text for explanation of dashed lines. a: Anterior; AA: anterior apex; Ap: aperture; Ch: channel; d: dorsal; p: posterior; NC: nasal cavity (outlined); PA: posterior apex; Pp: papilla; v: ventral; VA: ventral apex.

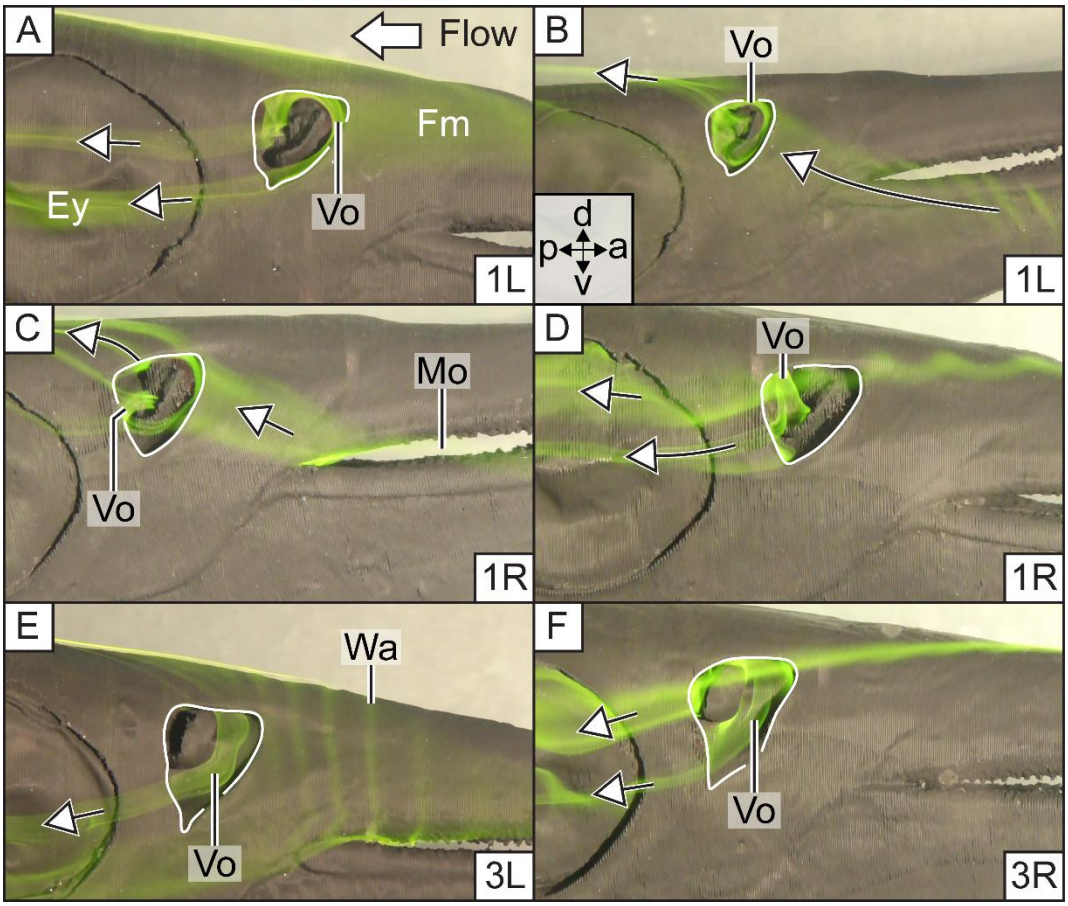

Fig. 8 Visualisation of flow in nasal regions of model garpike heads. Angle of attack and yaw: (A) 0°, 0°; (B) +10°, 0°; (C) +10°, 0°; (D) 0°, -10°; (E) 0°, -10°; and (F) 0°, -10°. Free-stream flow speed: 5 cm s^{-1}. Model (1, 2 or 3) and nasal region (left or right) designated in each panel, e.g. 1L is Model 1's left nasal region. White outlines: nasal cavities. Small white arrows: flow from or to nasal cavity. Large white arrow: direction of free-stream flow. a: Anterior; d: dorsal; Ey: eye; Fm: film of dye; Mo: gap in mouth; p: posterior; v: ventral; Vo: vortex-like structure; Wa: wave of dye.

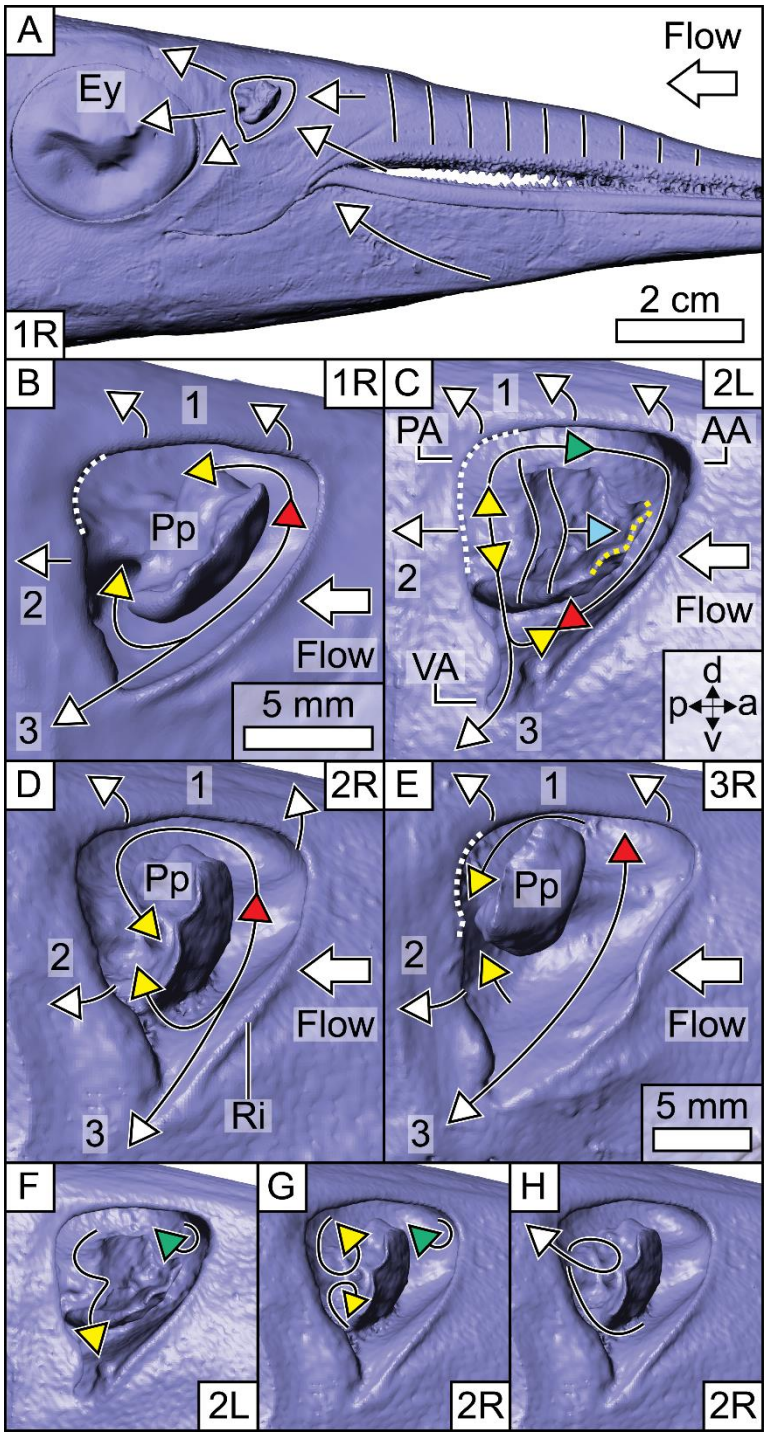

Fig. 9 Schematics of flow in the head and nasal regions of model garpike. (A) Flow in the head region. (B) – (E) Flow in the nasal regions. Model (1, 2 or 3) and nasal region (left or right) designated in each panel. (F) – (H): vortex-like structures in nasal regions. Small white arrows: flow from or into nasal cavity; large white arrows: direction of free-stream flow. For explanation of colour of other arrows, and numbers,

see main text. Scale bar in (B) also applies to panels (C) and (D). a: Anterior; AA: anterior apex; d: dorsal; Ey: eye; p: posterior; PA: posterior apex; Pp: papilla; Ri: ridge; v: ventral; VA: ventral apex.

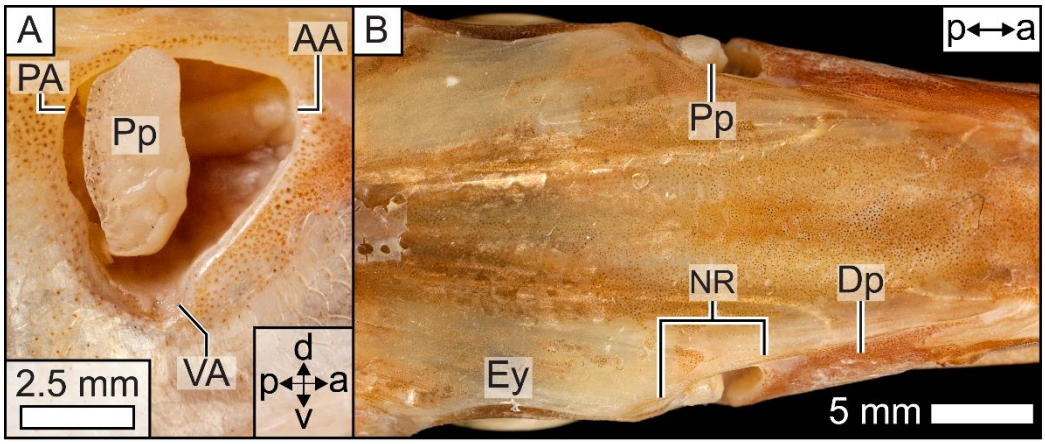

Fig. 10 Nasal regions of *Strongylura marina*, specimen BMNH 1939.7.10.14. (A) Right nasal region. (B) Dorsal aspect of head. a: Anterior; AA: anterior apex; d: dorsal; Dp: depression; Ey: eye; NR: nasal region; p: posterior; PA: posterior apex; Pp: papilla; v: ventral; VA: ventral apex.

Video legends

Video 1 Olfactory flow in model garpike. Model 1 (upside down); left nasal region; flow right to left; free-stream flow speed 5 cm s^{-1}; angle of attack 0°; yaw 0°. See also Fig. 8A.

Video 2 Olfactory flow in model garpike. Model 1 (upside down); left nasal region; flow right to left; free-stream flow speed 15 cm s^{-1}; angle of attack 0°; yaw 0°.

Video 3 Olfactory flow in model garpike, with dye flow from mouth. Model 1; right nasal region; flow right to left; free-stream flow speed 5 cm s^{-1}; angle of attack +10°; yaw 0°. See also Figs. 8C and 9B.

Video 4 Olfactory flow in model garpike. Model 1; right nasal region; flow right to left; free-stream flow speed 5 cm s^{-1}; angle of attack 0°; yaw -10°. See also Figs. 8D and 9B.

Video 5 Olfactory flow in model garpike. Model 2 (upside down); left nasal region; flow right to left; free-stream flow speed 5 cm s^{-1}; angle of attack 0°; yaw 0°. See also Fig. 9C.

Video 6 Olfactory flow in model garpike. Model 2 (upside down); left nasal region; flow right to left; free-stream flow speed 5 cm s^{-1}; angle of attack -10°; yaw 0°. See also Fig. 9C.

Video 7 Possible vortex in nasal region of model garpike. Model 2 (upside down); left nasal region; flow right to left; free-stream flow speed 15 cm s^{-1}; angle of attack 0°; yaw 0°. E.g. of possible vortex at 15 s. See also Fig. 9F.

Video 8 Olfactory flow in model garpike. Model 2; right nasal region; flow right to left; free-stream flow speed 5 cm s^{-1}; angle of attack 0°; yaw +10°. See also Fig. 9D.

Video 9 Possible vortex pair in nasal region of model garpike. Model 2; right nasal region; flow right to left; free-stream flow speed 20 cm s^{-1}; angle of attack 0°; yaw 0°. E.g. of possible vortex pair at 1 s. See also Fig. 9G.

Video 10 Possible vortex in nasal region of model garpike. Model 2; right nasal region; flow right to left; free-stream flow speed 15 cm s^{-1}; angle of attack +10°; yaw 0°. E.g. of possible vortex at 13 s. See also Fig. 9H.

Video 11 Olfactory flow in model garpike. Model 3 (upside down); left nasal region; flow right to left; free-stream flow speed 15 cm s^{-1}; angle of attack 0°; yaw 0°.

Video 12 Olfactory flow in model garpike. Model 3; right nasal region; flow right to left; free-stream flow speed 5 cm s^{-1}; angle of attack 0°; yaw -10°. See also Figs. 8F and 9E.